

Influence of Scandium on Corrosion Properties and Electrochemical Behaviour of Mg Alloys in Different Media

Ning Ma¹, Qiuming Peng^{1,*}, Xuejun Li¹, Hui Li¹, Jinghuai Zhang², Yongjun Tian¹

¹ State Key Laboratory of Metastable Materials Science and Technology, Yanshan University, Qinhuangdao, 066004, P.R China.

² Key Laboratory of Superlight Materials & Surface Technology, Harbin Engineering University,

*E-mail: pengqiuming@gmail.com

Received: 10 July 2012 / Accepted: 25 July 2012 / Published: 1 September 2012

Corrosion behaviour of Mg-xSc (x=0, 3, 5, wt.%) alloys prepared by zone purifying solidification technique has been investigated by immersion test and electrochemical measurement in both 0.9 wt.% NaCl solution and simulated body fluid. The results of immersion test show the corrosion resistance of Mg-3wt.%Sc alloy in both conditions is much higher than that of pure Mg or Mg-5wt.%Sc alloy. Moreover, the released hydrogen gas per day of Mg-3 wt.% Sc alloy is equivalent, which indicates that the corrosion process is homogeneous. Compared with pure Mg and Mg-5 wt.% Sc alloy, the oxide film is more uniform and compact. The oxide film includes Mg(OH)₂ and the sediment of Ca (H₂PO₄)₂ in simulated body fluid. The potentiodynamic polarization curves show that a current plateau is only observed in Mg-3wt.%Sc alloy due to the stable protective corrosion film. The electrochemical impedance spectroscopy curves of Mg-3wt.%Sc alloy are mostly composed of two capacitive loops in high and low frequency regions because of the existence of stable double-layer capacitance controlled by diffusion. It is demonstrated that the improved corrosion properties of Mg-3wt.%Sc alloy are essentially attributed to the reduction of the cores of pitting corrosion.

Keywords: Mg-Sc alloys; Weight loss; Corrosion properties; Electrochemical behaviour; Electrochemical impedance spectroscopy

1. INTRODUCTION

The main bottleneck in the application of Mg based structural materials or biomaterials lies in their too fast corrosion rate [1]. Therefore, the coatings, such as micro-arc oxidation[2], polymer [3], acid treatment [4] and the composite layer [5], have been performed to improve their corrosion properties. With the protection of the coatings, Mg alloys can be used as some potential structural components or biomaterial implants. Unfortunately, the corrosion rate is out of control because it is

accelerated as soon as the coatings are destroyed [6]. Additionally, as potential biomaterials, these coatings increase the potential toxicity. Too much cyto-compatibility experiments should be performed before the clinic test [7]. Therefore, how to improve the corrosion properties of Mg alloys becomes one of important issues to enlarge their applications.

It is well known that the corrosion properties of Mg alloys are closely associated with secondary phases and the impurities, such as Fe, Ni, Cu etc [8]. Hence, the key issue to improve the corrosion properties focuses on the decrement of these origins of corrosion. For example, the physical method can divide the compounds containing Fe, Ni or Cu from the matrix effectively due to the temperature gradient [9]. In addition, the rapid-solidified Mg-Zn-RE alloy exhibits high anti-corrosion properties with the elimination of secondary precipitates [10]. The addition of alloying element or $MgCl_2$ solvent is also confirmed as an effective approach to enhance the corrosion properties of Mg alloys [11]. Therefore, a strategy to improve the corrosion properties of Mg alloys is proposed with the combination of the above advantages [12]. Briefly, an addition of active alloying element reacts with the impurities, and then the formed precipitates are separated from the melt under high cooling rate during the solidification.

The addition of scandium (Sc) is selected in terms of the following twofold reasons. On the one hand, the alloying element of Sc has recently been found as an effective addition to improve the mechanical properties [13, 14]. Mg-Sc based alloy is regarded as a potential system to develop outstanding creep resistance of Mg alloy [15, 16]. The mechanical properties and age behaviour have been well investigated [17]. However, the corrosion rate and corrosion mechanism of Mg-Sc system are still unclear. On the other hand, the addition of a small amount of Sc is prone to form Fe-Sc compound during the melting process [18]. Whilst the element of Sc is homogeneously dispersed in Mg matrix in virtue of its high solubility [19]. Thus, the addition of Sc is a possible approach to improve the corrosion properties of Mg alloys. In the present work, the corrosion rate has been measured by immersion test and electrochemical method in both 0.9 wt.% NaCl solution and simulated body fluid (SBF) at ambient temperature. The corrosion mechanism has been determined based on electrochemical impedance spectroscopy (EIS) and scanning electron microscope (SEM). These results provide some implications to design new corrosion resistance of Mg-Sc based biomaterials in the future.

2. MATERIALS AND METHODS

2.1 Materials preparation

Mg-xSc (x=0, 3, 5, all compositions given in wt.%) alloys was prepared by zone solidification purifying method [9]. The alloys were prepared in a (tantalum: Ta) Ta-crucible protected by a mixture of CO_2 and SF_6 . After mixing at 720 °C for 1 hour, the alloy was cast to the mould preheated at 650 °C. The filled mould was held at 670 °C for 1 hour under the protective gas. Then, the whole Ta-crucible with the alloy was immersed into the cool water at 1 mm/s. When the bottom of Ta-crucible touched the water, it stopped for 2 seconds. As soon as the liquid level of inside melt was alignment

with the height of water outside, the solidification process was finished. The ingot of 60 mm in diameter and 180 mm in length was obtained. The chemical composition was studied by X-ray fluorescence spectroscopy, and the detailed composition was shown in Table 1.

Table 1. The detailed chemical composition of the alloys.

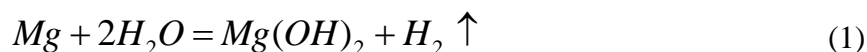
Alloys	Elements (wt.%)				
	Sc	Fe	Ni	Cu	Mg
Mg	-	<0.002	<0.001	<0.001	Bal.
Mg-3Sc	2.46	<0.003	<0.001	<0.001	Bal.
Mg-5Sc	4.51	<0.003	<0.001	<0.001	Bal.

2.2 Microstructure and microhardness

The microstructural investigations were performed using optical microscope (OM) and SEM equipped with energy dispersive X-ray spectrometry (EDX). The phase composition of the corrosion products was studied by X-ray diffraction (XRD) technique. For microstructural observation, the standard metallographic procedures were applied, including grinding, polishing and etching. The samples were etched in a picral solution to reveal grain boundaries. The grain size was measured using the linear intercept method. The microhardness test was carried out on a Vickers hardness tester, the test load and dwell time were 100 g and 15 s, respectively. The average value is determined by ten random spots.

2.3 Immersion test

For the immersion test, three replicated specimens were used for the alloy in each condition. Before testing, the specimen surfaces were polished, cleaned with alcohol solution, and then dried in warm flowing air. The corrosion rate was tested in 0.9 wt.% NaCl solution and SBF at ambient condition at a temperature of $25 \pm 1^\circ\text{C}$. The ratio of surface area to solution volume was $1 \text{ mm}^2 : 2 \text{ ml}$. The composition of SBF has been reported in our previous literature [20]. The tested time was two weeks. No external stirring was used. The corrosion reaction of Mg alloys was calculated by the following chemical equation [21-22]:



During the immersion test, the amount of released hydrogen gas (H_2) was recorded continuously. The average corrosion rate of each specimen at the end of the tests was calculated in millimeter per year by converting the total amount of collected hydrogen into materials loss ($1 \text{ ml H}_2 = 0.001083 \text{ g dissolved Mg}$) by means of the following equation (weight change Δg in g, surface area A in cm^2 , time t in hour, density of the alloy: ρ in g cm^{-3}) [12].

$$ACR = \frac{8.76 \times 10^4 \times \Delta g}{A \times t \times \rho} \quad (2)$$

2.4 Potentiodynamic polarization curve

Electrochemical tests were carried out using a Bio-logic VSP potentiostat/frequency response analysis system to evaluate the corrosion behaviors of the specimens at ambient condition at a temperature of $25 \pm 1^\circ\text{C}$. A electrode of Ag/AgCl (saturated with KCl) was used as the reference electrode. A platinum mesh and the investigated specimen were used as the counter electrode and the working electrode (3.96 mm^2 exposed area), respectively. The electrochemical tests were conducted in both 0.9 wt.% NaCl and SBF solutions at a scan rate of 0.25 mV/s. The polarization curves were used to estimate the corrosion and passivation potentials (E_{corr} , E_{pp}), and corrosion current density (I_{corr}) at corrosion potential (E_{corr}) by the Tafel extrapolation of the cathodic branch. Three samples have been performed to obtain the average result and the standard deviation. The I_{corr} , is related to the ACR (mm/y) using the conversion equation [23]:

$$ACR = 22.85 I_{\text{corr}} \quad (3)$$

2.5 Electrochemical impedance spectroscopy

The instrument and three electrodes were the same as the above electrochemical test. The EIS studies were performed at open circuit potential with the amplitude of 10 mV over the frequency range of 10,000-0.1 Hz on specimens exposed to the corrosive electrolyte for different durations viz., 2, 4, 6, 8 and 12 h to investigate the corrosion mechanism. All the tests were performed at ambient condition at a temperature of $25 \pm 1^\circ\text{C}$ with stirring in the bottom, and the tests were performed in triplicate to ascertain reproducibility.

3. RESULTS AND DISCUSSION

3.1 Microstructural characterization

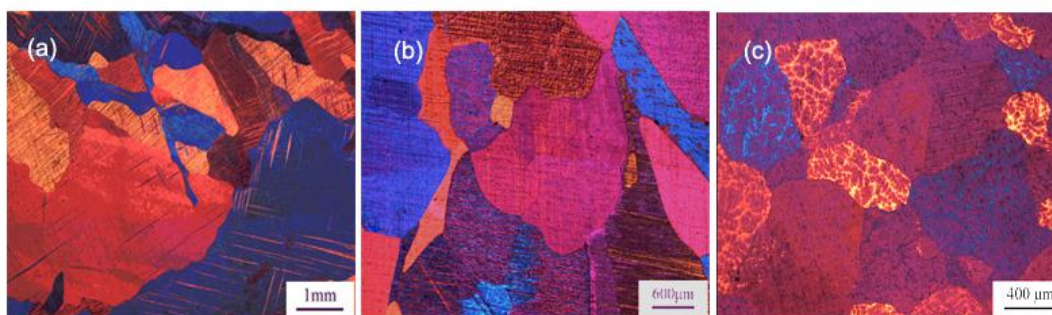


Figure 1. Optical micrographs of as-cast Mg-xSc alloys, (a) pure Mg; (b) Mg-3Sc alloy; (c) Mg-5Sc alloy

The microstructures of as-cast Mg-xSc alloys are shown in Fig. 1. In the case of pure Mg, the majority of grains are distributed along the temperature gradient direction and some twins are observed on the surface (Fig. 1a). The sample is composed of continuous grain boundaries and the matrix. Compared with pure Mg, Mg-3Sc alloy mostly consists of dendrites instead of twins. It reveals that the addition of Ce restrains the formation of twin during the polishing process, which is in agreement of the addition of Zn [20]. With further increasing the concentration of Sc, the secondary dendrites are more obvious and the grain size is decreased simultaneously. The average grain size of Mg-5Sc alloy is about 0.85 mm, which is only 35 percent as high as that of pure Mg.

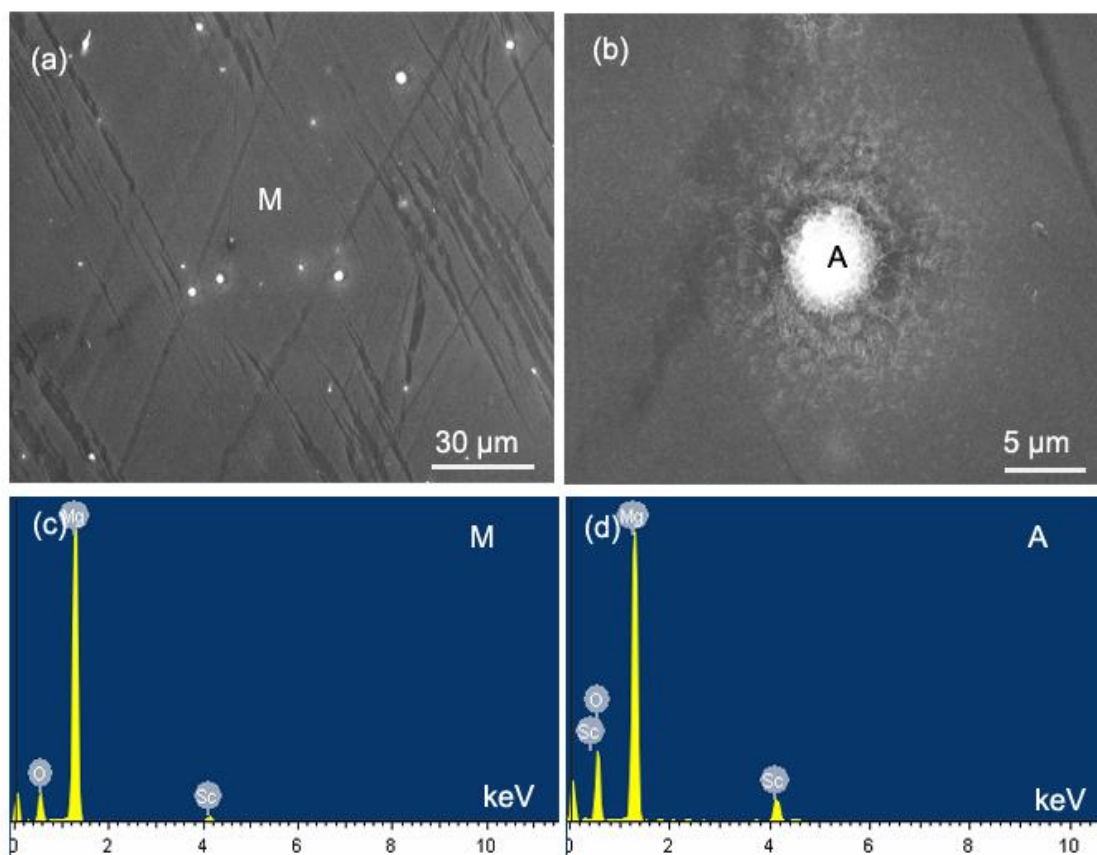


Figure 2. (a) SEM graph of as-cast Mg-5Sc alloy; (b) local high magnification of (a); (c) elemental composition of the matrix; (d) elemental composition of granular-shaped precipitate.

The representative SEM graphs of Mg-5Sc alloy are shown in Fig. 2. Some white globular particles are detected in the alloy. The dimension of globular precipitate is about 4.5 μm . The elemental compositions of both the matrix and the precipitate are shown in Fig. 2c and 2d, respectively. The concentration of Sc is 1.85 wt.% (0.97 at.%). The content of Sc in white globular precipitate is 73.21 wt.% (39.04 at.%). According to the phase diagram and our previous result [17], it can be confirmed that the precipitate is MgSc compound.

The concentration of Sc dependence on the microhardness is shown in Fig. 3. The microhardness of Mg-5Sc alloy is 46 HV, which is 1.21 times as high as that of pure Mg. The improved microhardness was mostly associated with the following two factors: firstly, the dilute solid

solution obeys *Friedel limit* that the concentration dependence of the yield stress varies as square root of solid solution concentration ($c^{-1/2}$)[24]. Namely, solid solution strengthening increases strength of the material by increasing the stress to move dislocations. The Sc element is well-dispersed in the Mg matrix.

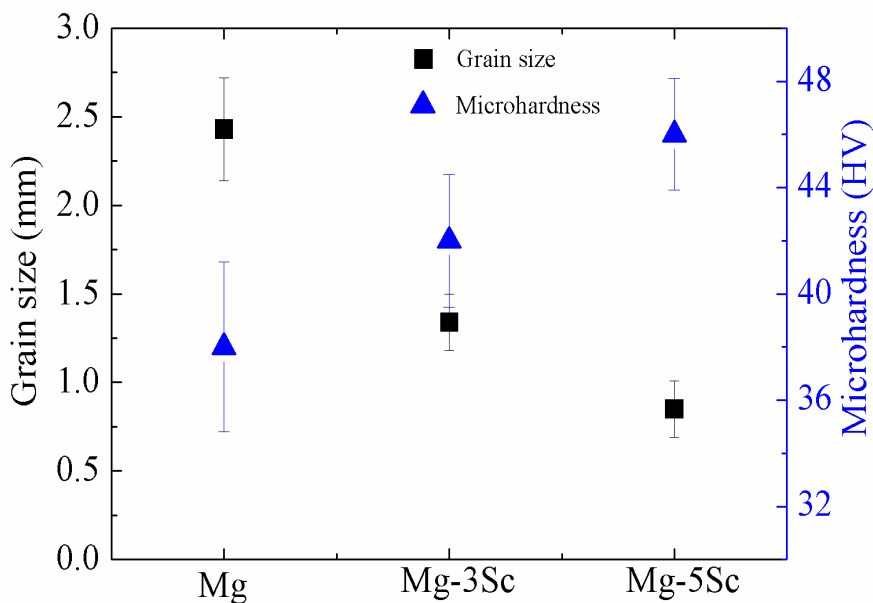


Figure 3. Grain size and microhardness of as-cast Mg-xSc alloys

Therefore, the microhardness is enhanced greatly. Secondly, the high microhardness is ascribed to fine microstructure. It is well recognized that a dislocation passing into the near grains or dendrites of different orientations has to change its direction of motion. Hence, the atomic disorder within a boundary region results in a discontinuity of slip planes from one to the other. The increased fraction of boundaries prevented the dislocation movement effectively (follows the essence of Hall-Petch relationship [25]).

3.2 Immersion test

3.2.1 Evaluation by hydrogen gas

The typical trends of the content of H_2 in SBF solution are shown in Fig. 4. For pure Mg sample, the volume of H_2 is about 2 ml per day. Compared with pure Mg and Mg-5Sc alloy, the amount of released H_2 per day of Mg-3Sc alloy is the lowest. Furthermore, as far as Mg-3Sc alloy is concerned, the fluctuation of released H_2 per day is minimum. The value is between 1.5 and 1.7 ml every 24 hours. On the contrary, the amount of released H_2 varies greatly in Mg-5Sc alloy. The value of released H_2 is about 1.8 ml at the beginning, and it changes to 4.9 ml after immersed for nine days.

The detailed corrosion rate of Mg-xSc alloys in different solutions is shown in Fig. 5. The average corrosion rate of pure Mg is about 1.71 mm/y in 0.9 wt.% NaCl solution. However, the value changes to 1.32 mm/y in SBF solution. The corrosion rate of Mg-3Sc alloy in 0.9 wt.% NaCl solution and SBF is 1.12 and 0.91 mm/y, respectively. The immersion test shows that Mg-xSc alloys exhibit higher corrosion resistance in SBF than that in 0.9 wt.% NaCl solution.

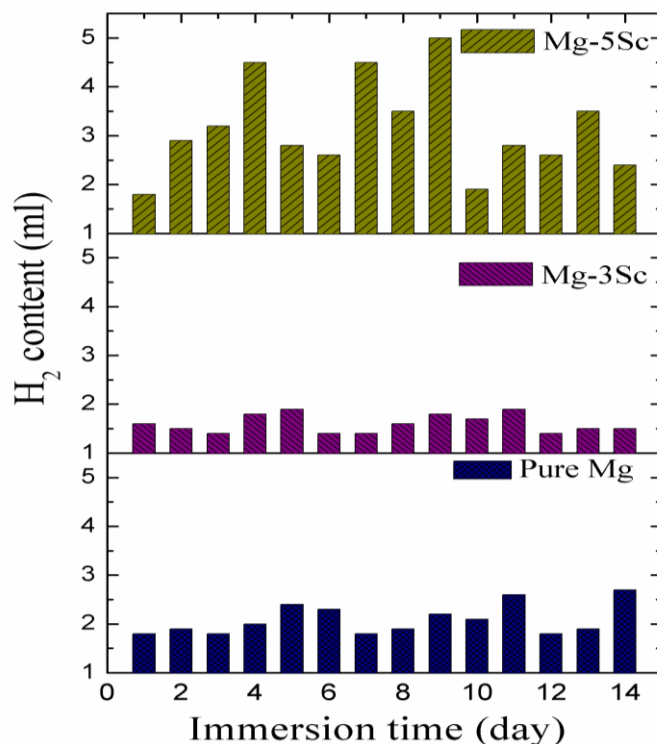


Figure 4. The representative relationship between released hydrogen gas and immersion time in SBF solution.

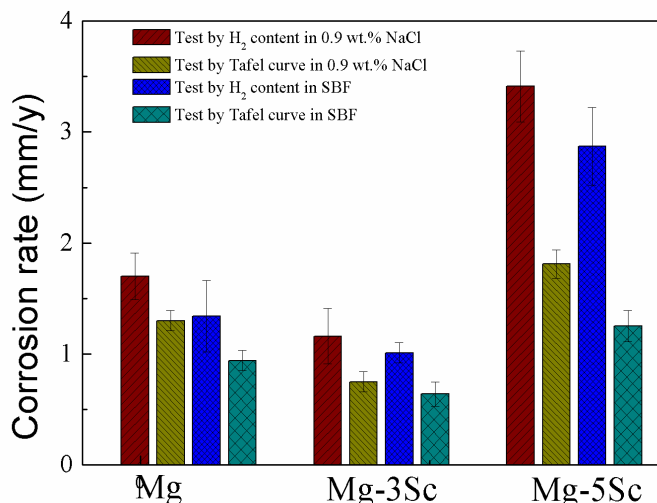


Figure 5. Average corrosion rate of Mg-xSc alloys in different solution at ambient temperature based on immersion test and electrochemical method.

In addition, it is established that the addition of 3 wt.%Sc can effectively improve the corrosion properties. Particularly, it offers a corrosion rate in 0.95 mm/y in SBF solution (the prerequisite of Mg based implant is less than 1 mm/y). There are two factors accounting for the above phenomenon. On the one hand, Sc is very active element in Mg alloys, which is prone to form Fe_2Sc compound (enthalpy of formation: -34 kJ/mol [18]). Thus, the concentration of Fe in the melt is reduced greatly with the formation of Fe_2Sc precipitate, which is deposited in the bottom owing to its higher density. The explanation was verified by the chemical composition (Table 1). Due to the decrement of the impurities, the corrosion properties of Mg-3Sc alloy are improved greatly. On the other hand, according to Mg-Sc binary phase diagram [19], it can be found that Mg-3Sc is mostly composed of single phase solid solution. Thus, the pitting corrosion is eliminated without the formation of secondary precipitate. Therefore, the low and stable corrosion rate is obtained. The similar result is reported in Mg-Y alloy [26], namely, the corrosion properties of Mg-Y alloy is enhanced with increasing the solid solution in Mg matrix under high pressure solidification.

3.2.2 Appearance and corrosion products

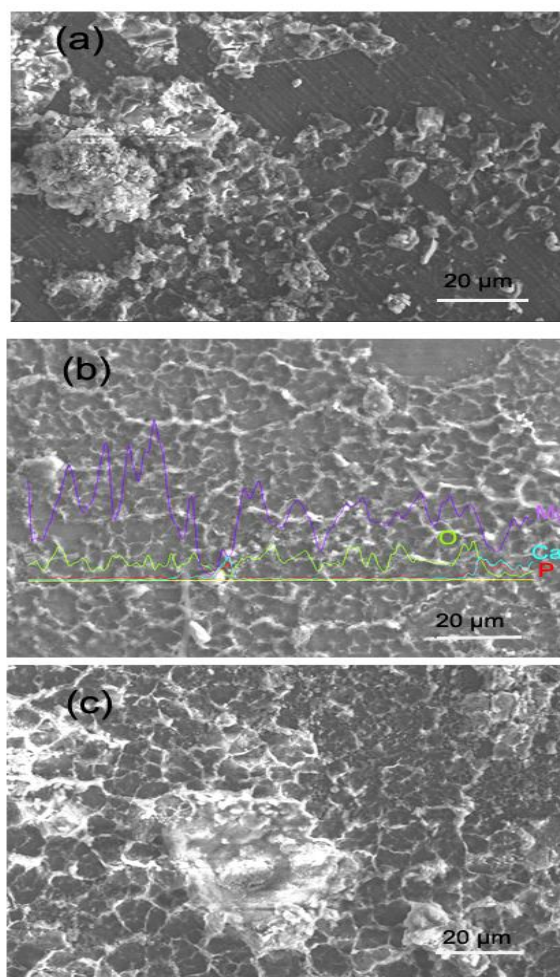


Figure 6. Morphologies after immersion in SBF for 7 days, (a) pure Mg; (b) Mg-3Sc alloy; (c) Mg-5Sc alloy.

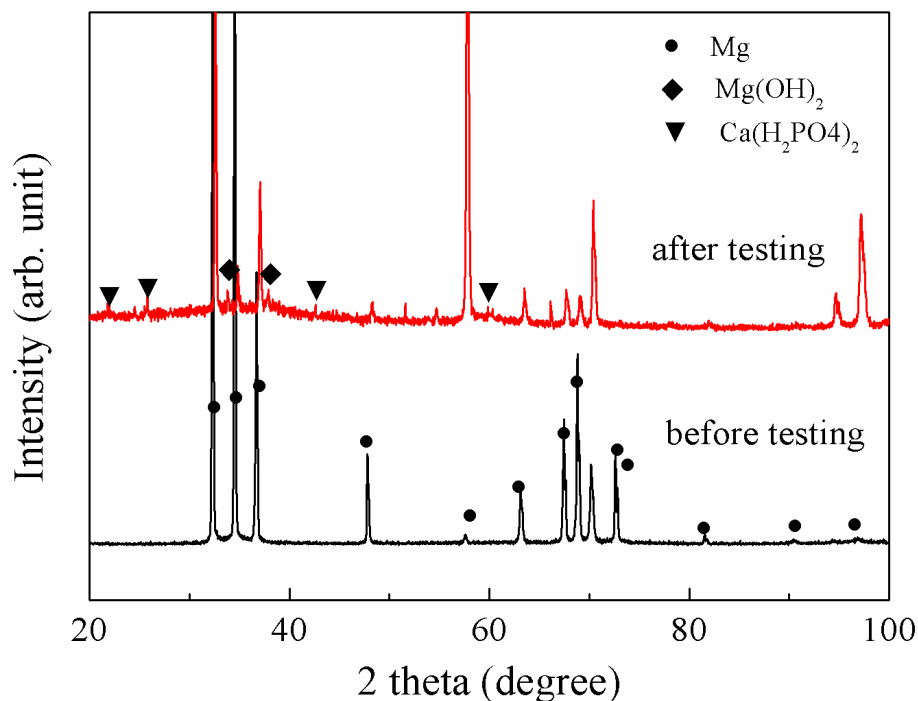


Figure 7. XRD patterns of Mg-3Sc alloy before and after immersed in SBF solution for 14 days.

After the samples are immersed in SBF for 7 days, the specimen surface was covered with a film of corrosion products. The specimen surfaces after the immersion test are shown in Fig. 6. Some flocculent oxides are segregated on the surface of pure Mg (Fig. 6a). Moreover, the film is discontinuous and loose. At the same time, some cracks are clearly observed on the surface, which are the channels to release H_2 . In the case of Mg-3Sc sample, the net-shaped oxide film is very compact. The film (white area) is mostly composed of the elements of Ca, P, Mg and O without other impurities. On the contrary, some large pits are detected in Mg-5Sc alloy. Moreover, the whole surface is loose. There are some honeycomb-shaped holes on the surface. It reveals that pitting corrosion is dominated the corrosion process.

The XRD patterns of Mg-3Sc before and after immersion test in SBF are shown in Fig. 7. It can be seen that Mg-3Sc curve before immersion chiefly consists of Mg peaks, which demonstrates that the alloy is mostly composed of solid solution. Conversely, after immersion test, some additional peaks of both $Mg(OH)_2$ and $Ca(H_2PO_4)_2$ are observed in Mg-3Sc alloy. It indicates that the corrosion product of Mg-3Sc is $Mg(OH)_2$. At the same time, the $Ca(H_2PO_4)_2$ compound is also accumulated on the surface during the immersion test.

According to the previous results [27, 28], the corrosion products of Mg alloy present a three-layered structure, generally characterized by a hydrated inner $MgO-Mg(OH)_2$ layer, a dense thin intermediate MgO region and an outer porous layer containing $Mg(OH)_2$ formed by a dissolution-precipitate mechanism. In our investigation, the oxide film of Mg-3Sc alloy is compact and uniform and it is mostly composed of $Mg(OH)_2$ and $Ca(H_2PO_4)_2$. The element of Sc is absolutely dissolved in the solution. MgO peaks are not observed partially owing to the little amount on the surface, which can

not be detected by means of XRD. Mg-Zn-Ca based biomaterial also exhibits the similar corrosion process [29, 30].

3.3 Electrochemical behaviour

3.3.1 Potentiodynamic polarization curves

Potentiodynamic polarization curves (named Tafel curves) of Mg-xSc alloys in both SBF and 0.9 wt.% NaCl solution are shown in Fig. 8.

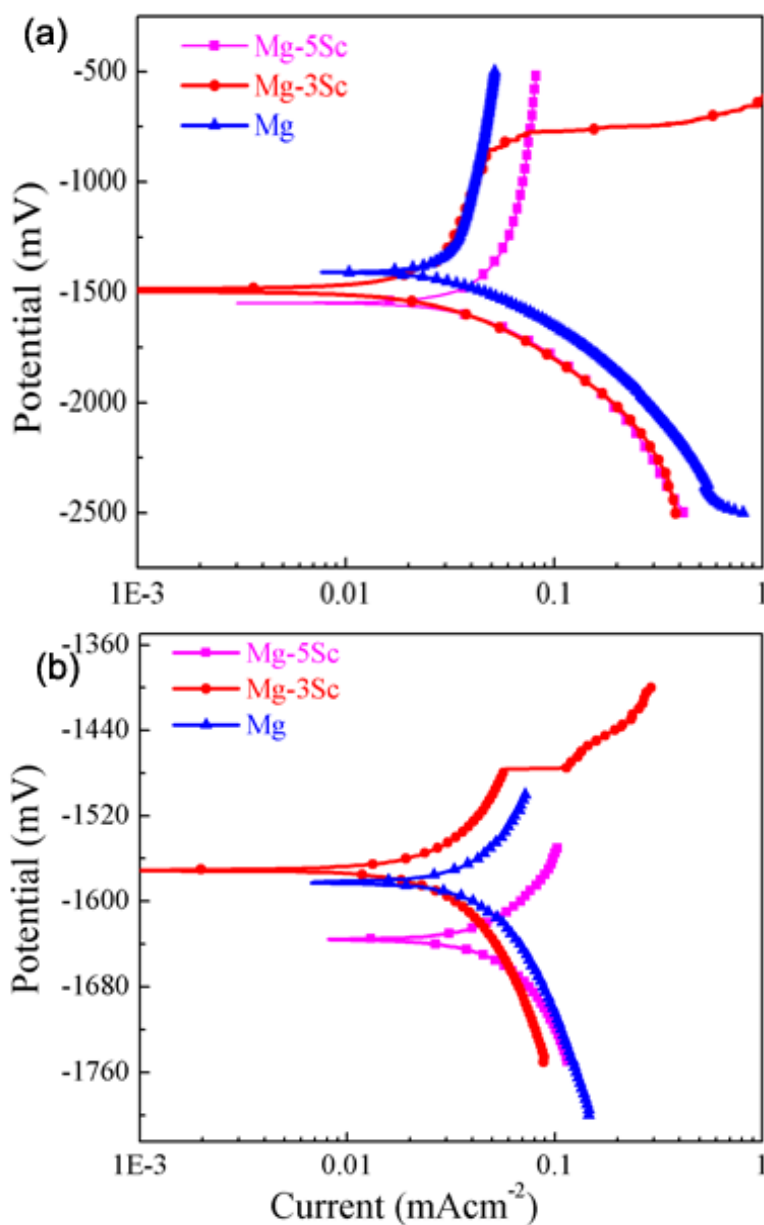


Figure 8. Tafel curves of Mg-xSc alloys in different solutions, (a) SBF solution; (b) 0.9 wt.% NaCl.

Table 2. Electrochemical parameters of the samples derived from polarization tests in 0.9 wt.% NaCl and SBF solutions at ambient temperature.

Environment	Alloys	E_{corr} (mV)	I_{corr} (mA/cm ²)	E_{pp} (mV)
SBF	Mg	-1401	4.13×10^{-2}	-
	Mg-3Sc	-1489	2.81×10^{-2}	-824
	Mg-5Sc	-1554	5.47×10^{-2}	-
0.9 wt% NaCl	Mg	-1583	5.69×10^{-2}	-
	Mg-3Sc	-1569	3.28×10^{-2}	-1477
	Mg-5Sc	-1637	7.91×10^{-2}	-

The detailed values deduced from the polarization curves are listed in Table 2. With increasing the concentration of Sc, the polarization curves shift toward negative direction in SBF. Namely, the E_{corr} is decreased with the addition of Sc in SBF (Fig. 8a). The E_{corr} of pure Mg is -1401 mV (Ag/AgCl), and it varies to -1554 mV (Ag/AgCl) in Mg-5Sc alloy. The I_{corr} of Mg-3Sc is 2.81×10^{-2} mA/cm², which is 51 percent as high as that of the Mg-5Sc alloy. The similar trend that the I_{corr} is reduced by adding Sc is also observed in 0.9 wt.% NaCl solution. The only discrepancy is that the I_{corr} in 0.9wt.% NaCl solution is higher than that in SBF. In addition, the passivation plateau ($\Delta E = E_{\text{pp}} - E_{\text{corr}}$) is about 665 mV, which is 7.23 times higher than that in 0.9 wt.% NaCl. It also indicates that the corrosion resistance properties of Mg-xSc alloy in SBF are better than those in 0.9 wt.% NaCl solution.

The corrosion rates calculated based on Tafel curves are also shown in Fig. 5. The similar trend as that measured by immersion test is observed. Generally, the corrosion rate in 0.9 wt.% NaCl solution is higher than that in SBF solution correspondingly. For instance, the corrosion rate of Mg-5Sc alloy calculated from Tafel curve is 1.8 mm/y in 0.9 wt.% NaCl solution, which is 1.63 times as high as that in SBF. Meanwhile, it should be mentioned that the value of 0.65 mm/y is observed for the Mg-3Sc alloy in SBF.

3.3.2 Electrochemical impedance spectroscopy

The Nyquist plots of Mg-xSc alloys after immersion in 0.9 wt.% NaCl solution for time up to 12 hours are shown in Fig. 9. Three samples exhibit the similar trend during the whole investigated range. It is found that the curves are mainly composed of two capacitive loops in high and low frequencies (HF and LF) regions during all the immersion range. Moreover, the radius is increased with increasing the immersion time. In addition, the effects of the immersion time in SBF solution on the Nyquist plots of Mg-xSc alloys are shown in Fig. 10. Three samples show different EIS behaviours. For pure Mg, the curve is mostly composed of two capacitive loops (HF and LF) and an inductive loop (LF) when the immersed time is less than 4 hours. However, the EIS curve chiefly concludes a capacitive loop (HF) and an inductive loop (LF) when the immersion time is over than 4 hours. On the contrary, all EIS curves of Mg-3Sc alloy are composed of two capacitive loops (HF and LF) and an inductive loop (LF). All EIS curves of Mg-5Sc alloy contain both a capacitive loop (HF) and an inductive loop (LF).

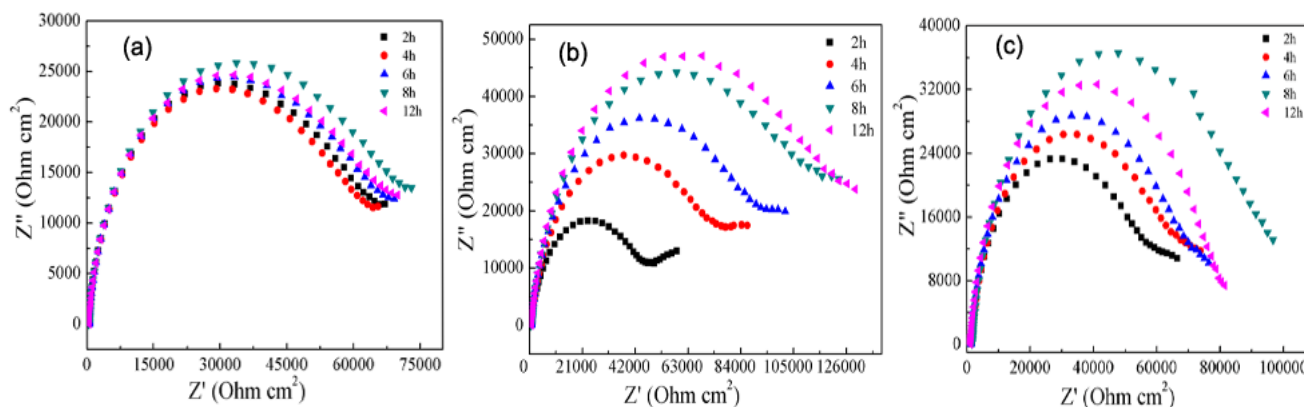


Figure 9. EIS curves in 0.9 wt.% NaCl after different immersion time, (a) pure Mg; (b) Mg-3Sc alloy; (c) Mg-5Sc alloy.

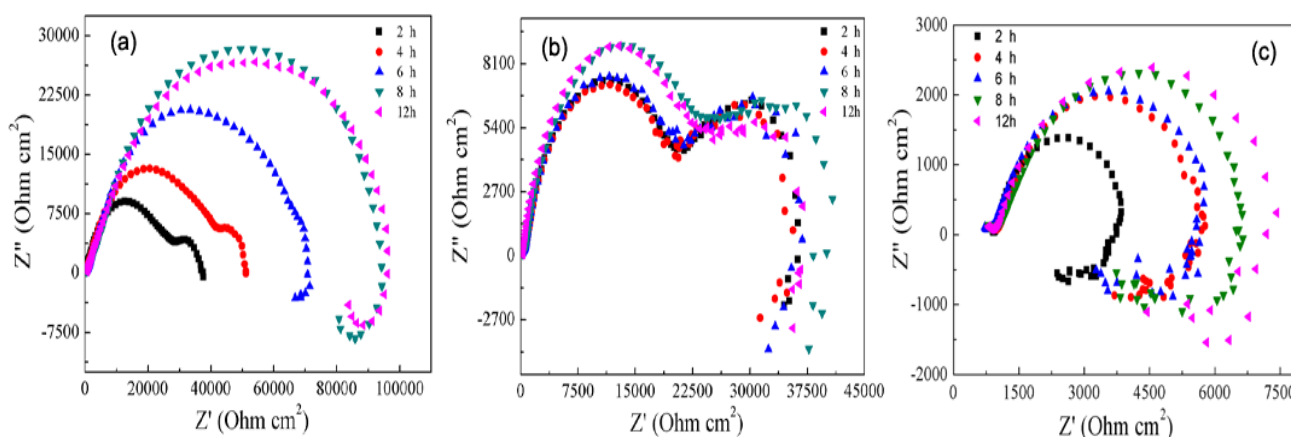


Figure 10. EIS curves in SBF solution after different immersion time, (a) pure Mg; (b) Mg-3Sc alloy; (c) Mg-5Sc alloy.

The EIS results demonstrate that Mg-xSc alloys exhibit different corrosion mechanisms. It is well known that a HF capacitive loop is mostly associated with the double layer capacitance at the solution/metal interface [21]. The capacitive loop at low frequency is generally attributed to the film-free areas controlled by diffusion [26]. The existence of an inductive loop at low frequency is related to the pitting corrosion [8]. Three possible equivalent circuits are shown in Fig. 11. For pure Mg, the fitting plots can be represented as $R_s(C_1R_{ct})(C_2R_w)$ (Fig. 10a) when the immersion time is less than 4 hour. However, it changes to $R_s(C_1(R_{ct}(C_2R_x)))$ (Fig. 10c) as the immersion time further increases. On the contrary, during the whole investigated range, the fitting circuits of Mg-3Sc and the Mg-5Sc alloys are $R_s(C_1R_{ct})(C_2(R_wR_L))$ (Fig. 9b) and $R_s(C_1(R_{ct}(C_2R_x)))$ (Fig. 9c), respectively. R_s and R_{ct} are solution resistance and charge transfer resistance, respectively. C and R_L stand a capacitance and an inductance, respectively. R_x is related to the new pitting corrosion resistance. At the same time, the radius is generally increased with increasing the immersion time, which demonstrated that the width of the

oxide film is increased and the anti-corrosion properties is improved correspondingly. The same corrosion behaviors have been reported in Mg-Y and Mg-Sr alloys [31-33].

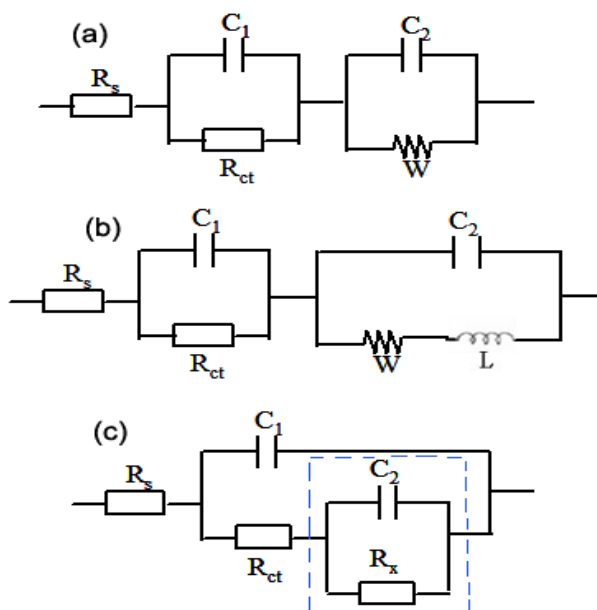


Figure 11. Fitting equivalent circuits in 0.9 wt.% NaCl solution and SBF.

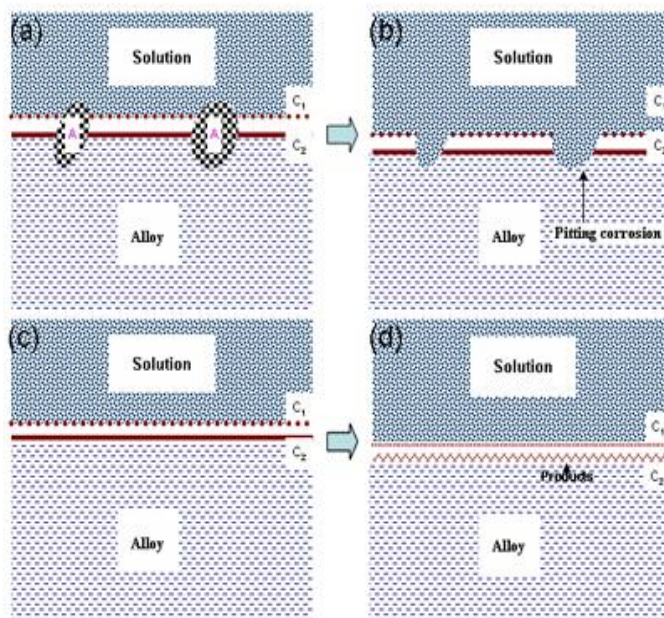


Figure 12. Schematic corrosion mechanisms of as-cast Mg-xSc alloys in SBF solution; (a) and (b) Mg and Mg-5Sc alloy; (c) and (d) Mg-3Sc alloy.

The representative schematic diagrams of corrosion process are shown in Fig. 12. For pure Mg, it can be elucidated that the stable double layer controlled by diffusion is readily formed on the surface at the beginning corrosion. Whereas the diffusion layer is destroyed and the solution penetrates the film when the immersion time is over 4 hour. Accordingly, the pitting corrosion forms due to the existence of Fe impurity (marked A, in Fig. 12a), which accelerates the corrosion process. Similarly, the existence of MgSc precipitate (Fig. 3) breakdowns the oxide film readily in the Mg-5Sc alloy. Thus, the pitting corrosion emerges when the alloy is immersed into the solution (Fig. 12a and 12b). On the contrary, the uniform double electron layer and diffusion layer produces when the Mg-3Sc alloy is immersed into the solution. The continuous and compact oxide film is homogeneously distributed on the surface (Fig. 12c and 12d). Therefore, with the elimination of the impurities and secondary particle [34], Mg-3Sc alloy exhibits outstanding anti-corrosion properties in both 0.9 wt.% NaCl solution and SBF.

4. CONCLUSIONS

In summary, the effect of Sc on the corrosion properties and electrochemical behaviour of Mg alloys in both 0.9 wt.% NaCl solution and SBF have been studied by means of immersion test and electrochemical method. The addition of 5 wt.% Sc refines the grain size from 2.43 to 0.85 μm . The hardness is improved from 38 to 46 HV. The amount of released hydrogen gas per day is stable in Mg-3Sc alloy. The average corrosion rate of Mg-3Sc alloy by immersion test and electrochemical method is 0.95 and 0.65 mm/y in SBF solution, respectively. The improved corrosion properties of Mg-3Sc alloy are closely related to the formation of continuous and compact oxide film. The mainly corrosion product on the surface is $\text{Mg}(\text{OH})_2$ compound. It is confirmed that the removal of the heterogeneous particles (Fe impurity and MgSc compound) is a critical factor to enhance the corrosion properties of Mg-Sc based alloys.

ACKNOWLEDGEMENTS

This research is financially supported by National Natural Science Foundation of China (Grant No. 51101142 and 50821001) and Postdoctoral Science Foundation (2012M510766). The authors thank Dr. Daqing Fang and Dr. Hanwu Dong for stimulating discussion.

References

1. F. Czerwinski, Magnesium Alloys - Design, Processing and Properties, Rijeka: InTech, 2011.
2. L. Zhao, C. Cui, Q. Wang, S. Bu, *Corr. Sci.* 52 (2010) 2228.
3. J. Li, Y. Song, S. Zhang, C. Zhao, F. Zhang, X. Zhang, L. Cao, Q. Fan, T. Tang, *Biomaterials*. 31 (2010) 5782.
4. A. De Witte, E. De Maeyer, R. Verbeeck, *Biomaterials*. 24 (2003) 1995.
5. H. Duan, K. Du, C. Yan, F. Wang, *Electrochem. Acta*. 51 (2006) 2898.
6. F. Czerwinski, Magnesium Injection Molding, New York:Springer, 2008.
7. F. Feyerabend, J. Fischer, J. Holtz, F. Witte, R. Willumeit, H. Drücker, C. Vogt, N. Hort, *Acta*

- Biomater.* 6 (2010) 1834.
8. G. Song, Corrosion of magnesium alloys, Cambridge: Woodhead, 2011.
 9. Q. Peng, Y. Huang, L. Zhou, N. Hort, K. Kainer, *Biomaterials*. 31 (2010) 398.
 10. M. Yamasaki, N. Hayashi, S. Izumi, Y. Kawamura, *Corr. Sci.* 49 (2007) 255.
 11. E. Emley, Principle of Magnesium Technology, New York: Pergamon, 1966.
 12. K. Kainer, Magnesium, Weinheim: Wiley-VCH, 2009.
 13. B. Mordike, *Mater. Sci. Eng. A.* 324 (2002) 103.
 14. B. Smola, I. Stulikova, F. von Buch, B. Mordike, *Mater. Sci. Eng. A.* 324 (2002) 113.
 15. A. Rudajevova, F. von Buch, B. Mordike, *J. Alloys Compd.* 292 (1999) 27.
 16. F. von Buch, J. Lietzau, B. Mordike, A. Pisch, R. Schmid-Fetzer, *Mater. Sci. Eng. A.* 263 (1999) 1.
 17. Q. Peng, N. Ma, X. Li, J. Zhang, *Mater. Lett.* 78 (2012) 58.
 18. X. Liu, P. Yu, C. Wang, K. Ishida, *J. Alloys Compd.* 466 (2008) 169.
 19. M. Avedesian, H. Baker, ASM Specialty Handbook: Magnesium and Magnesium Alloys, Materials Park, OH: ASM International, 1999.
 20. Q. Peng, X. Li, N. Ma, R. Liu, H. Zhang, *J. Mech. Behav. Biomed. Mater.* 10 (2012) 128.
 21. G. Song, A. Atrens, *Adv. Eng. Mater.* 5 (2003) 837.
 22. ASTM-G31-72, American Society for Testing and Materials: Standard practice for laboratory immersion corrosion testing of metals, 2004.
 23. M. Zhao, M. Liu, G. Song, A. Atrens, *Corr. Sci.* 50 (2008) 3168.
 24. R. Arsenault, S. Patu, D. Esterling, *Mater. Trans. A.* 20A (1989) 1411.
 25. L. Friedman, D. Chrzan, *Phy. Rev. Lett.* 81 (1998) 2715.
 26. Q. Peng, S. Zhao, H. Li, N. Ma, X. Li, Y. Tian, *Int. J. Electrochem. Sci.* 7 (2012) 5581.
 27. J. Nordlien, K. Nisancioglu, S. Ono, N. Masuko, *J. Electrochem. Soc.* 143 (1996) 2564.
 28. S. Ono, H. Kijima, N. Masuko, *Mater. Trans.* 44 (2003) 539.
 29. C. Janning, E. Willbold, C. Vogt, J. Nellesen, A. Meyer-Lindenberg, H. Windhagen, F. Thorey, F. Witte, *Acta Biomater.* 6 (2010) 1861.
 30. B. Zberg, P. Uggowitzer, J. Löffler, *Nature Mater.* 8(2009) 887
 31. M. Liu, P. Schmutz, P. Uggowitzer, G. Song, A. Atrens, *Corr. Sci.* 52 (2010) 3687.
 32. A. Sudholz, K. Gusieva, X. Chen, B. Muddle, M. Gibson, N. Birbilis, *Corr. Sci.* 53 (2011) 2277.
 33. H. Brar, J. Wong, M. Manuel, *J. Mech. Behav. Biomed. Mater.* 7 (2011) 87.
 34. Q. Peng, Y. Huang, K. Kainer, N. Hort, *Adv. Eng. Mater.* 14 (2012) 178.